Simulation study on the cross section measurement of $e^+e^- \to \pi^+\pi^-\pi^0$ through the radiative return method at Belle II

Yuki Sue[*]

Graduate School of Science, Nagoya University, Nagoya 464-8602, Japan

Abstract

This note presents plots of MC study for the cross section measurement of $e^+e^- \to \pi^+\pi^-\pi^0$:

- Signal efficiency [Fig. 1]

- Variable distributions for cuts: χ^2_{4C} [Fig. 2], and the background reduction cuts [Figs. 3–6]

- The di-photon invariant mass $M(\gamma\gamma)$ distributions and their fits [Fig. 7]

- Fitting variable distributions for tracking efficiency correction [Fig. 8]

- Fitting variable distributions for π^0 efficiency correction [Figs. 9 and 10]

- The three-pion invariant mass $M(3\pi)$ resolution [Fig. 11]

- The distribution of the response function used for unfolding [Fig. 12]

- The expected signal spectrum and the luminosity-scaled main background event distribution [Fig. 13]

The study is based on the internal note [1] and event selection is summarised in Table I. MC samples are run-independent MC14.
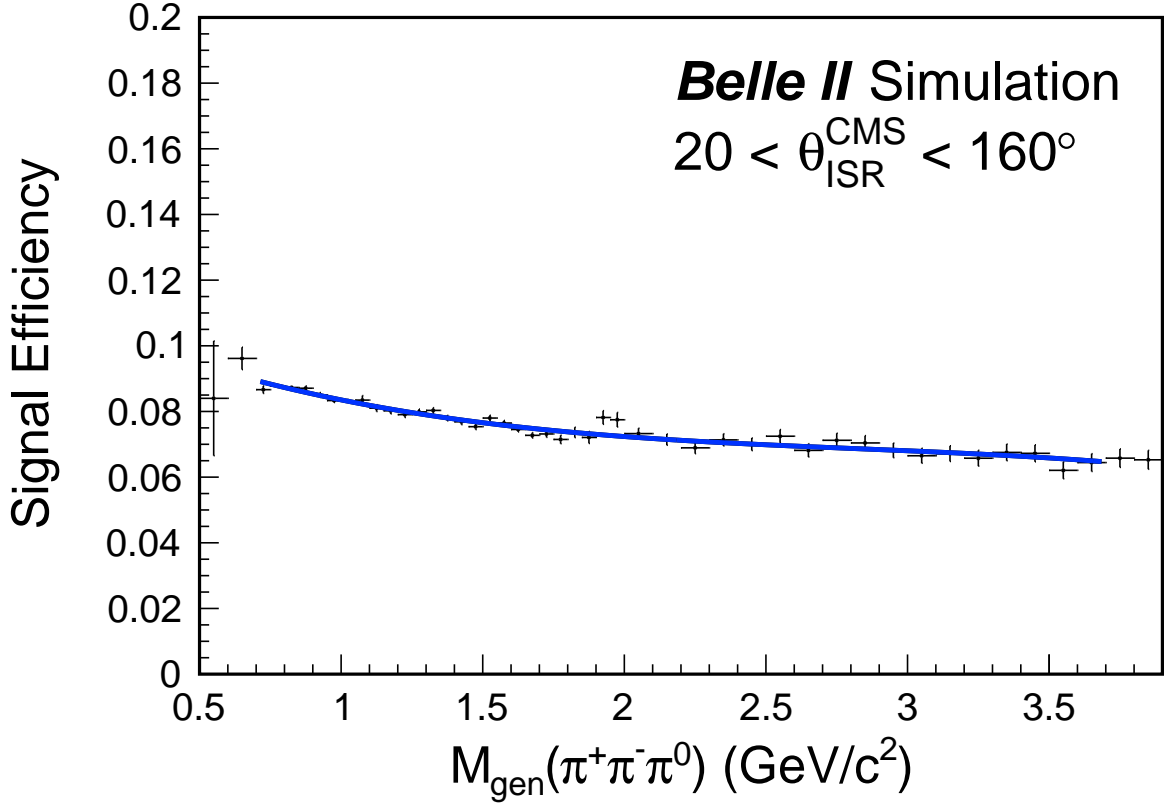
[*] ysue@hepl.phys.nagoya-u.ac.jp

FIG. 1: Detection efficiency dependence on the generated invariant mass of $\pi^+\pi^-\pi^0$ using $e^-e^- \to \pi^+\pi^-\pi^0\gamma$ MC. The generated event, denominator, is required to have the invariant mass of $\pi^+\pi^-\pi^0\gamma$ is more than 8 GeV and a ISR photon whose energy is more than two GeV and the polar angle is within 20 to 160 degree in the centre-of-mass frame. The blue line shows the result of fitting with a quintic function.
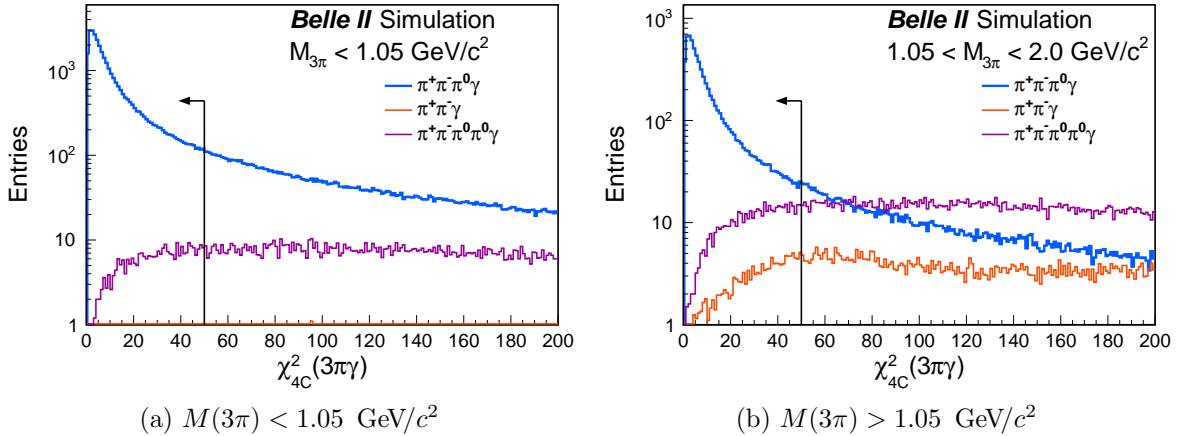

(a) $M(3\pi) < 1.05$ GeV/c^2

(b) $M(3\pi) > 1.05$ GeV/c^2

FIG. 2: The χ^2 distribution of four-momentum conservation kinematic fit under $e^+e^- \to \pi^+\pi^-\pi^0\gamma$ hypothesis to MC samples. The blue line shows the $e^+e^- \to \pi^+\pi^-\pi^0\gamma$ MC, the red line shows $e^+e^- \to \pi^+\pi^-\gamma$ MC, and the violet line shows $e^+e^- \to \pi^+\pi^-\pi^0\pi^0\gamma$ MC.
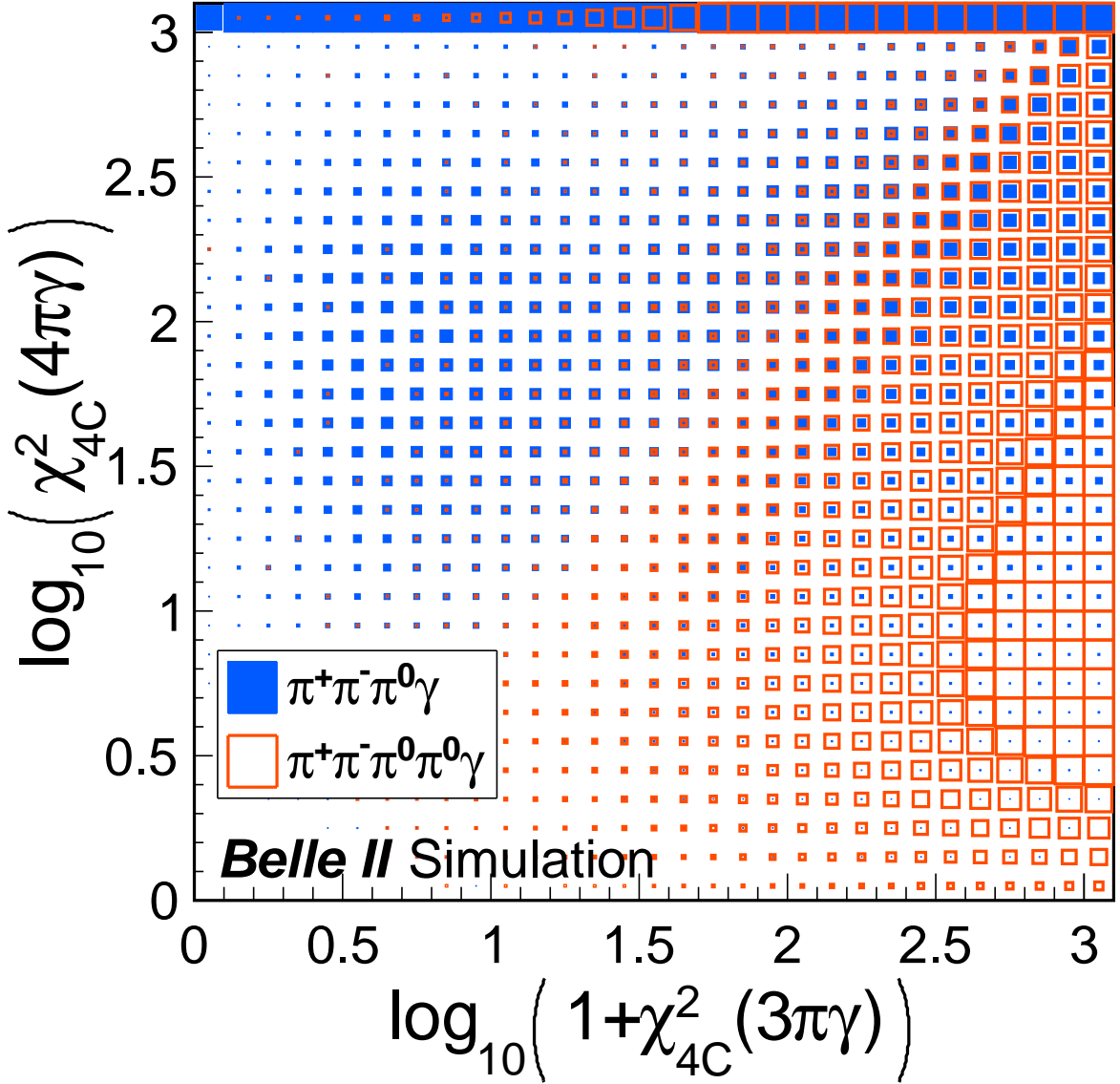
FIG. 3: The χ^2 distribution of four-momentum conservation kinematic fit under $e^+e^- \to \pi^+\pi^-\pi^0\gamma$ hypothesis (horizontal axis) and $e^+e^- \to \pi^+\pi^-\pi^0\pi^0\gamma$ hypothesis (vertical axis). The blue area shows $e^+e^- \to \pi^+\pi^-\pi^0\gamma$ MC, and red square shows $e^+e^- \to \pi^+\pi^-\pi^0\pi^0\gamma$ MC. The area indicates the number of events of MC samples. The top row shows the events where an additional π^0 is not found and $\pi^+\pi^-\pi^0\pi^0\gamma$ candidates cannot be reconstructed.
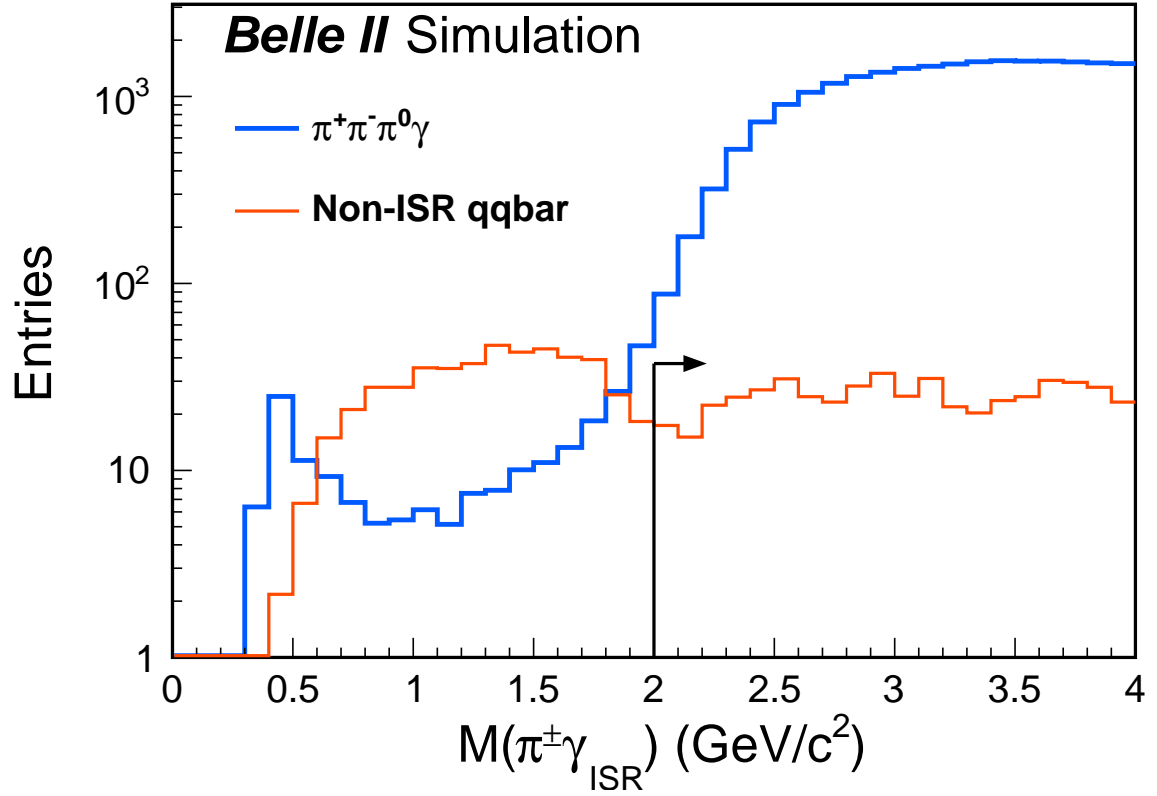
FIG. 4: The invariant mass distribution of charged pion and initial-state radiation photon (ISR). The blue histogram shows $e^+e^- \to \pi^+\pi^-\pi^0\gamma$ MC, and red one shows non-ISR $e^+e^- \to q\bar{q}$ MC.
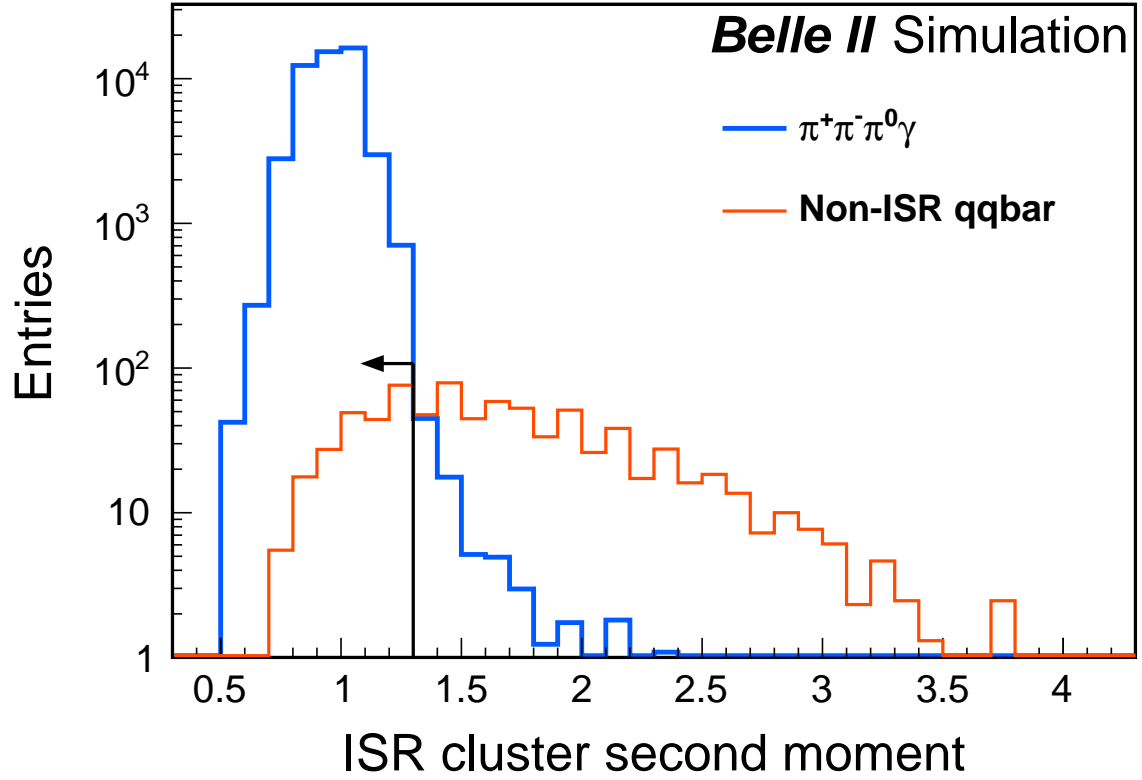
FIG. 5: The cluster second moment distribution of initial-state radiation photon (ISR). The cluster second moment is a moment of cluster aria weighted by a crystal energy, which is defined as $S = \frac{\sum_i^n E_i r_i^2}{\sum_i^n E_i}$ where i is the index of crystal, E_i is the single crystal energy, and r_i is the distance of the i-th digit to the shower centre projected to a plane perpendicular to the shower axis [2]. The blue histogram shows $e^+e^- \rightarrow \pi^+\pi^-\pi^0\gamma$ MC, and red one shows non-ISR $e^+e^- \rightarrow q\bar{q}$ MC.
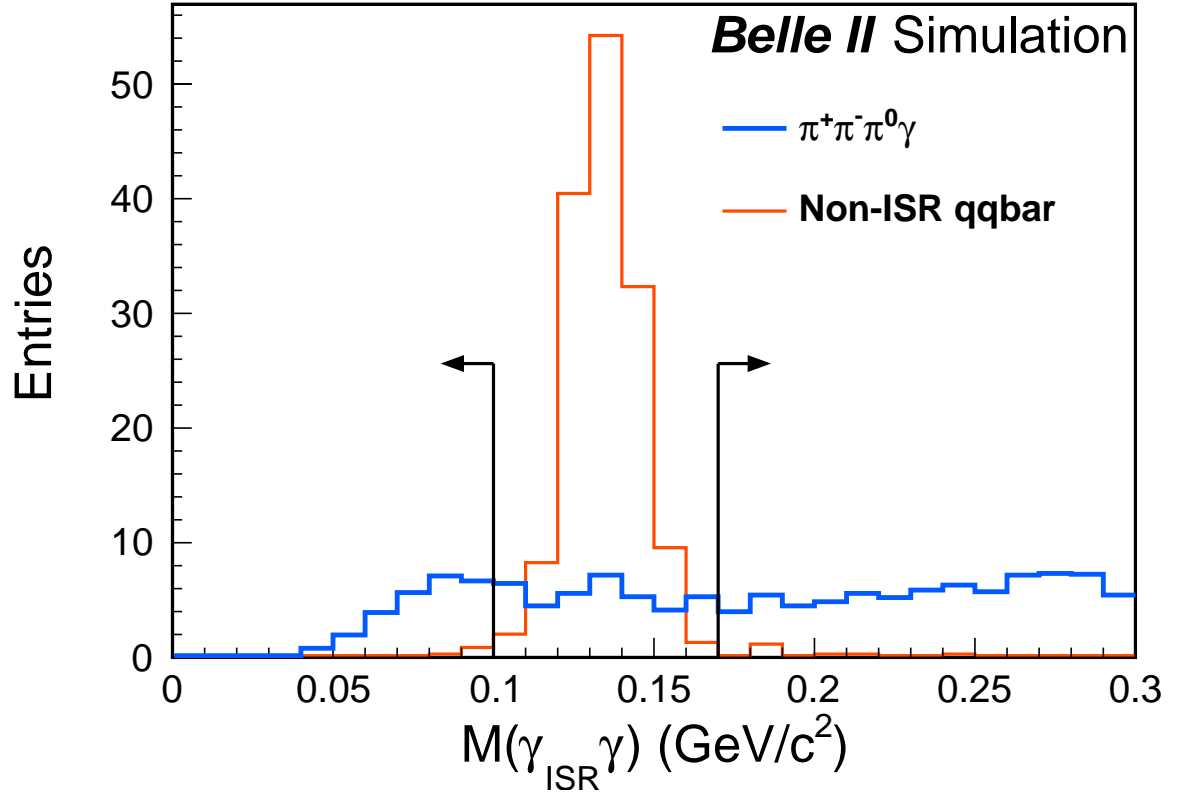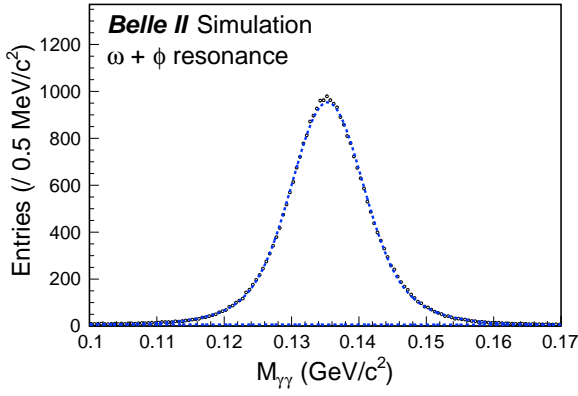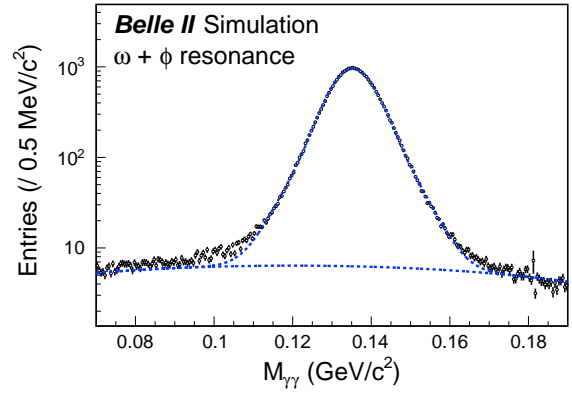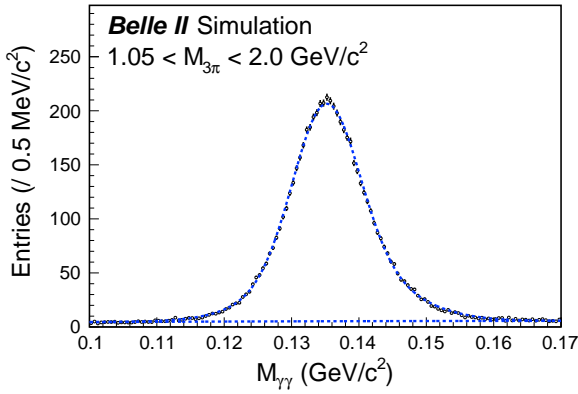
FIG. 6: The invariant mass distribution of initial-state radiation photon (ISR) and an additional photon. The blue histogram shows $e^+e^- \to \pi^+\pi^-\pi^0\gamma$ MC, and red one shows non-ISR $e^+e^- \to q\bar{q}$ MC.

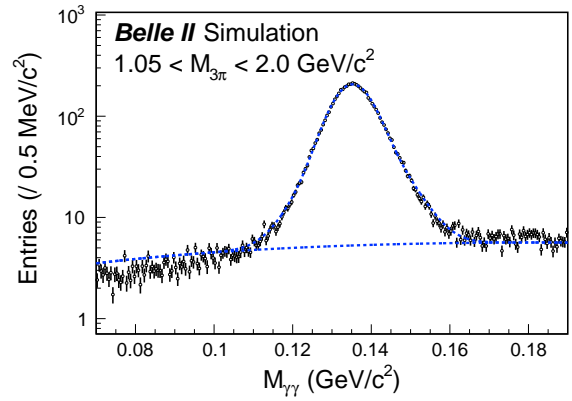(a) ω and ϕ resonance

(b) ω and ϕ resonance (log-scale)

(c) $1.05 < M(3\pi) < 2.0$ GeV/c^2

(d) $1.05 < M(3\pi) < 2.0$ GeV/c^2 (log-scale)

FIG. 7: The di-photon invariant mass distribution of $\pi^+\pi^-\pi^0\gamma$ signal events at the ω resonance. Each plots show different $M(3\pi)$ mass region, the right plots show the log-scale. The broken histogram shows the fit result. The signal pdf is modelled by the Novosibirsk function and single Gaussian, and the background pdf is the quadratic function.
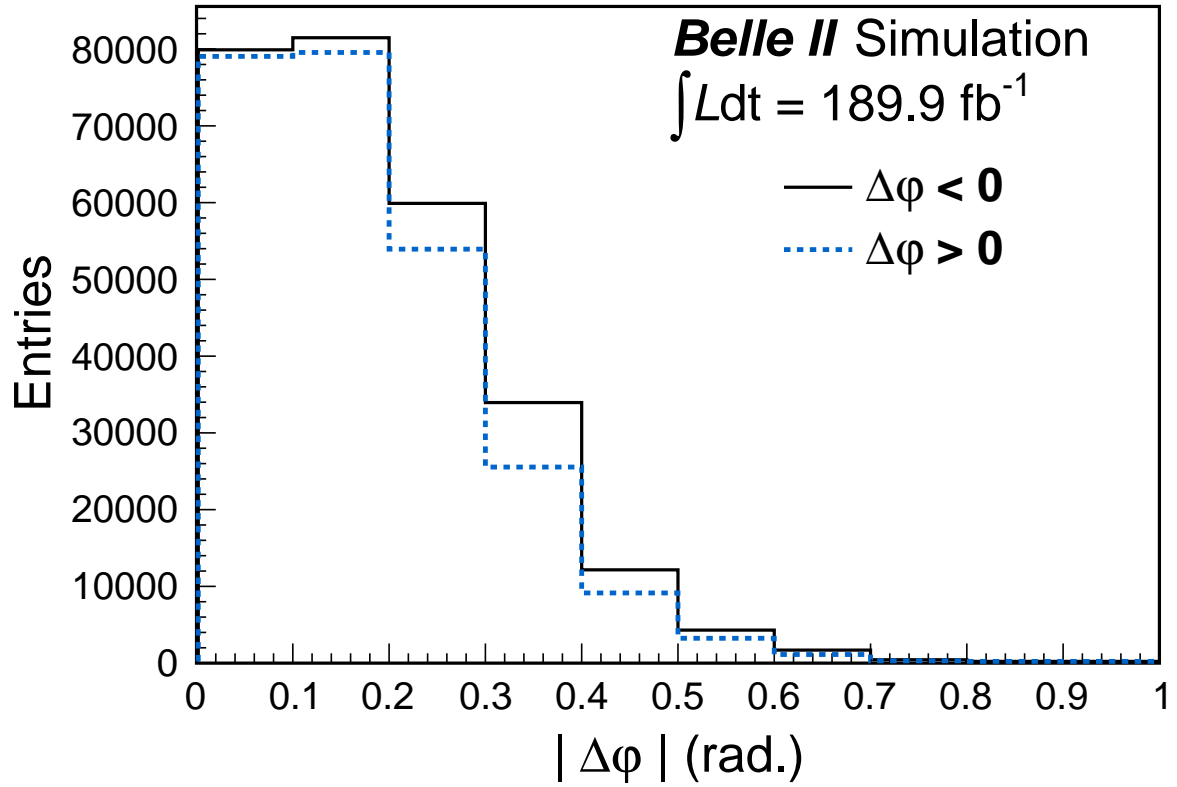
FIG. 8: The $|\Delta\varphi|$ distribution of $\pi^+\pi^-\pi^0\gamma$ signal at the ω resonance. The lines indicate $\Delta\varphi < 0$ events (solid) and $\Delta\varphi > 0$ (dashed) of $e^+e^- \to \pi^+\pi^-\pi^0\gamma$ MC. $|\Delta\varphi|$ difference between $\Delta\varphi < 0$ and $\Delta\varphi > 0$ expected in MC is also observed in the data, which is not plotted, and both are in good agreement except the smallest bin of $|\Delta\varphi| = 0$.
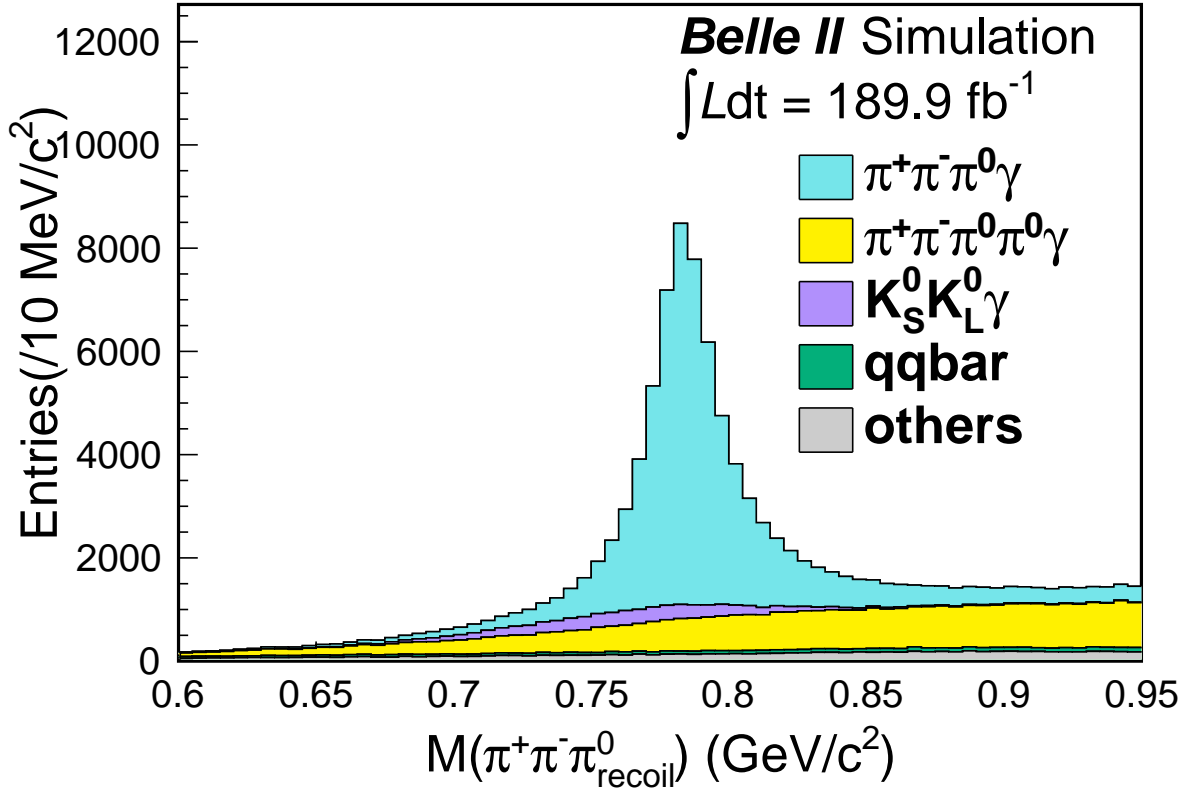
FIG. 9: The $M(\pi^+\pi^-\pi^0_{\mathrm{recoil}})$ distribution of the partial-reconstructed sample for the π^0 efficiency study. The $M(\pi^+\pi^-\pi^0_{\mathrm{recoil}})$ is calculated from the four vector of charged pions and the recoil momentum after a kinematic fit to $\pi^+\pi^-\gamma$ with a constrain of the recoil mass to be the π^0 mass. The stacked histograms are MC samples scaled by the integrated luminosity.
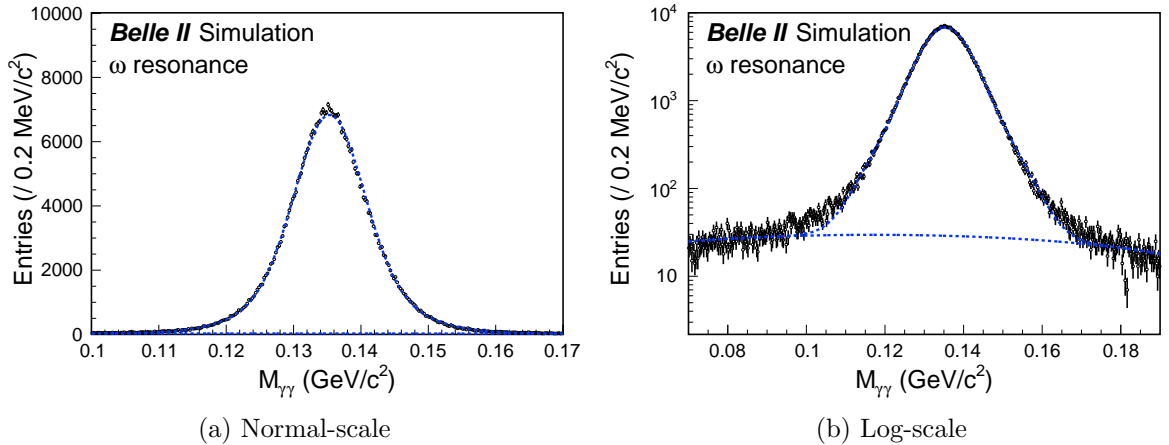

(a) Normal-scale

(b) Log-scale

FIG. 10: The di-photon invariant mass distribution of the full-reconstructed sample for the π^0 efficiency study. The broken histogram shows the fit result. The signal pdf is modelled as the Novosibirsk function and single Gaussian, and the background pdf is the quadratic function.
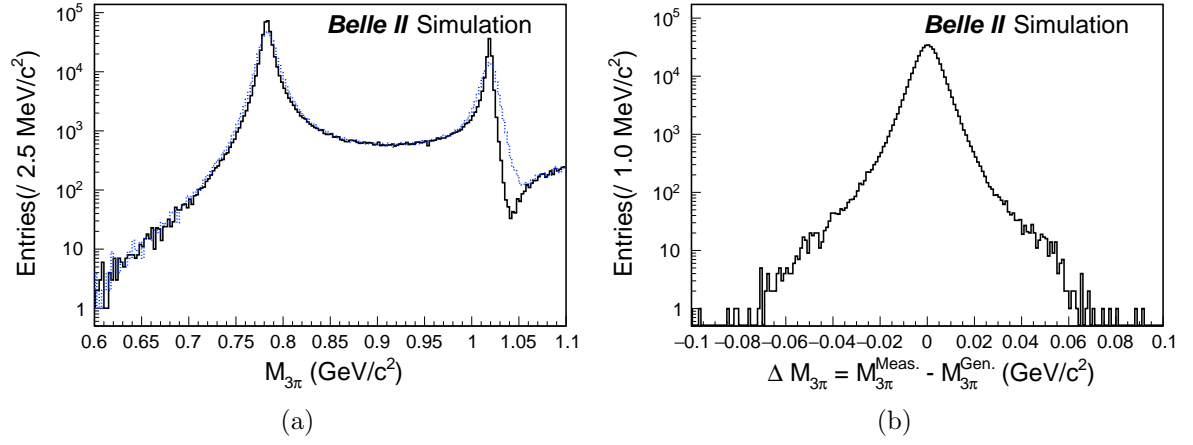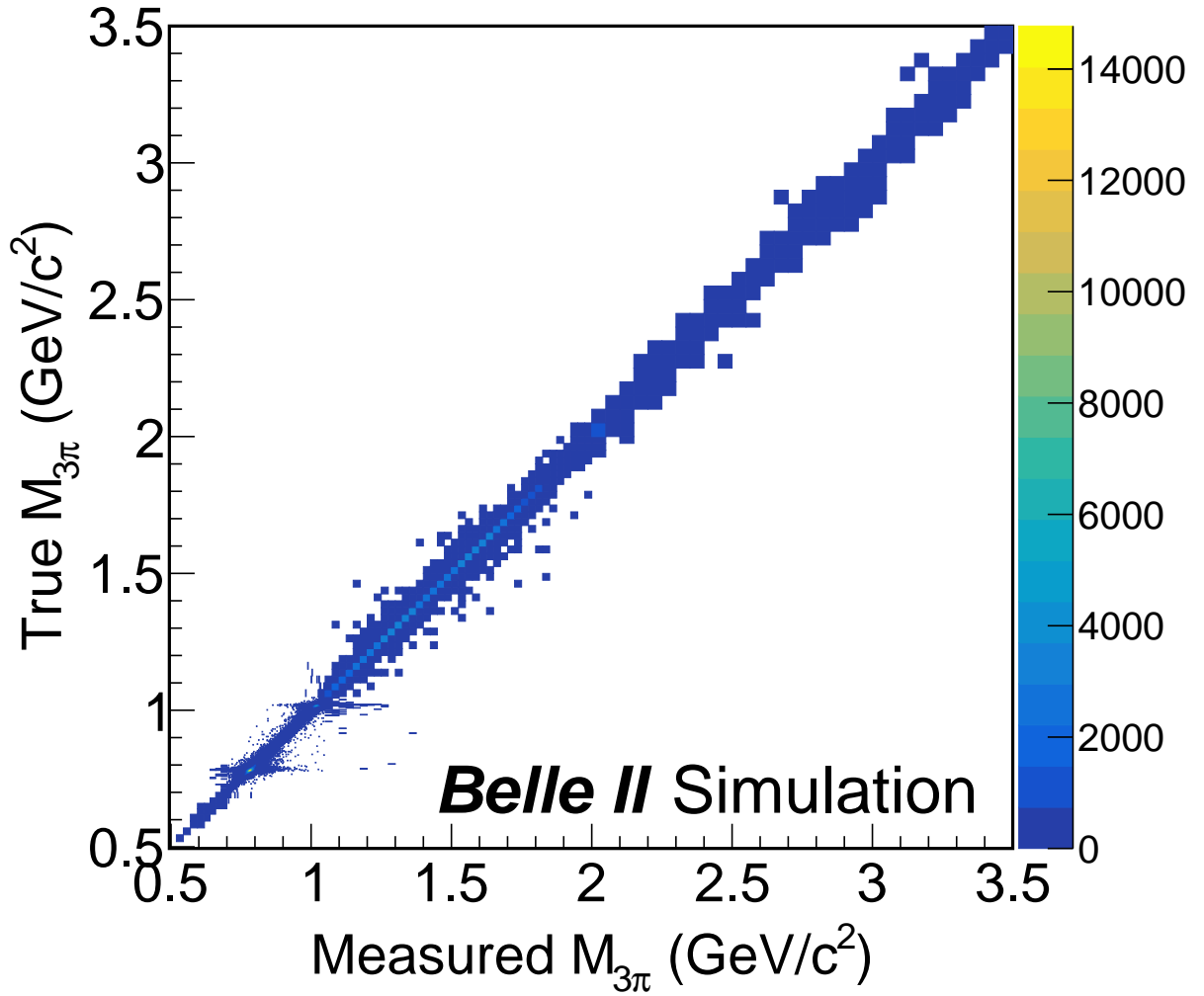
FIG. 11: (a) $M(\pi^+\pi^-\pi^0)$ spectrum of measured (solid) and generated values (dashed) of $e^+e^- \to \pi^+\pi^-\pi^0\gamma$ MC. (b) Difference of measured and generated values of $M(3\pi)$.

(a) $0.5 < M(3\pi) < 3.5$ GeV/c^2
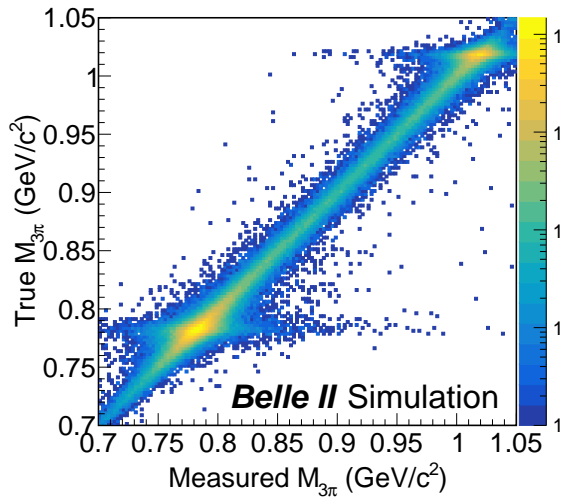
(b) $0.7 < M(3\pi) < 1.05$ GeV/c^2
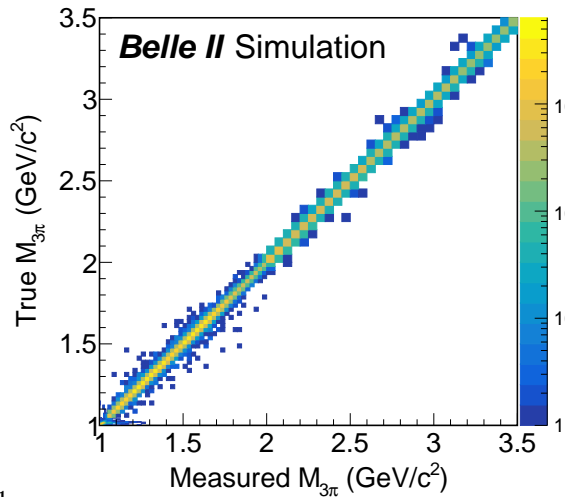
(c) $1 < M(3\pi) < 3.5$ GeV/c^2

FIG. 12: The scatter plots between measured (horizontal) and generated (vertical) values of $M(3\pi)$ in different mass regions.
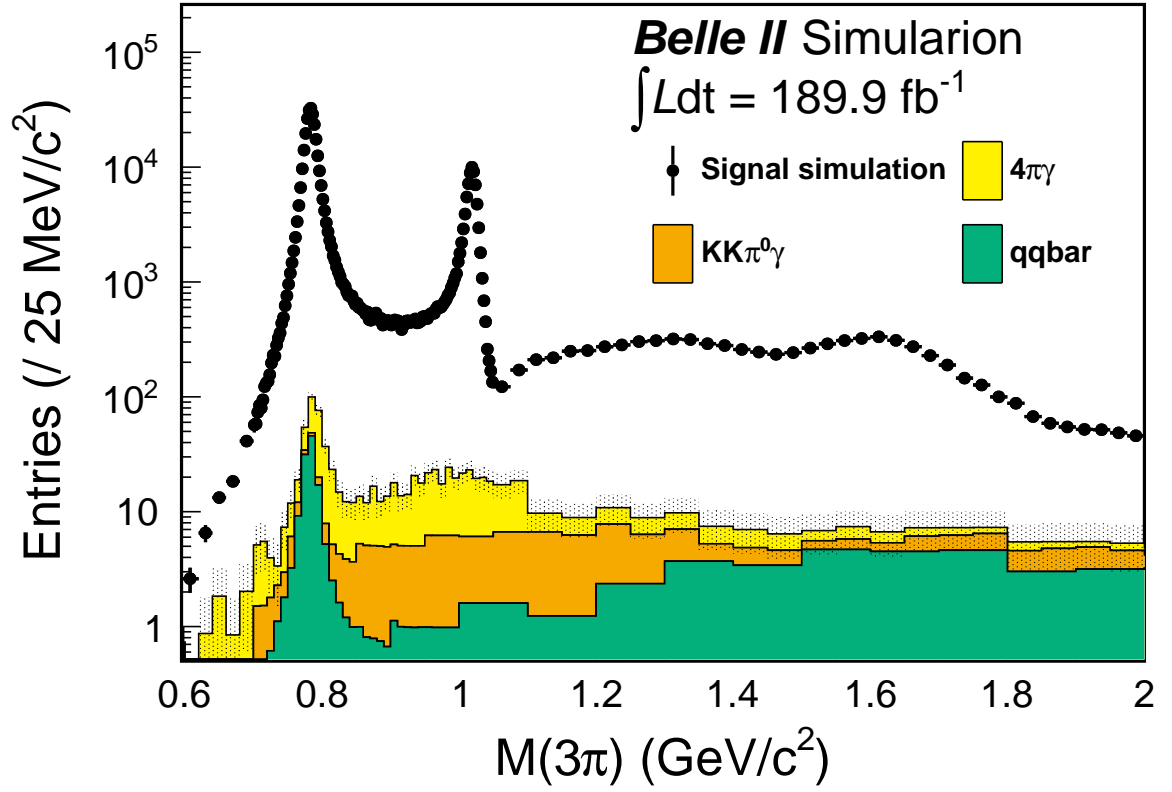
FIG. 13: The $M(3\pi)$ spectrum of the extracted signal and background MC. The dots with error bars show the signal obtained by $M(\gamma\gamma)$ fit to each $M(3\pi)$ bin. The stacked histogram is estimated backgrounds scaled by the luminosity. The number of entries in each bin is scaled to the 25 MeV/c^2 bin width.

TABLE I: The summary of standard selection for signal event.

Quantity	Cut
Tracks	
Transverse momentum	$p_T^{\text{lab}} > 0.2\,\text{GeV}$
Polar angle	$17.0 < \theta^{\text{lab.}} < 150°$
Vertex	$dr < 0.5\,\text{cm}$ and $|dz| < 2\,\text{cm}$
CDC hits count	nCDCHits > 20
$\gamma(\pi^0)$	
ECL cluster count	clusterNHits > 1.5
ECL cluster polar angle	$17 < \theta^{\text{lab.}}_{\text{cluser}} < 150°$
Energy	$E > 100\,\text{MeV}$
Event basis	
Tracks count	$N_{\text{track}} == 2$
Event charge	$\Sigma Q_{\text{track}} == 0$
Gamma count	$N_{\text{gamma}} \geq 3$
ISR photon	
CMS energy	$E^{\text{CMS}} > 2\,\text{GeV}$
Polar angle	$37.3 < \theta^{\text{lab.}} < 123.7°$
π^0 (after 4C-KFit)	
Invariant mass	$0.123\,\text{GeV} < m(\gamma\gamma) < 0.147\,\text{GeV}$
Daughter opening azimuthal angle	$|\Delta\phi| < 1.5\,\text{rad}$
Daughter opening angle	daughterAngle $< 1.4\,\text{rad}$
$\pi^+\pi^-\,\pi^0\,\gamma$	
Invariant mass	$M(\pi^+\pi^-\pi^0\gamma) > 8$ GeV
Four-conservation KFit χ^2	$\chi^2_{4\text{C},3\pi\gamma} < 50$
Background rejection	
Binary electron veto	$L_{\pi/e} > 0.1$
Binary kaon veto	$L_{\pi/K} > 0.1$
$\pi^+\pi^-\pi^0\pi^0\gamma$ rejection	$\chi^2_{4\text{C},4\pi\gamma} > 30$
$q\bar{q}$ rejection	$M(\pi^{\pm}\gamma) > 2\,\text{GeV}$
$q\bar{q}$ rejection	$M(\gamma_{\text{ISR}}\gamma) < 0.11$ GeV or $M(\gamma_{\text{ISR}}\gamma) > 0.17$ GeV
$q\bar{q}$ rejection	Cluster second moment $S_{\text{ISR}} > 1.3$
$\pi^+\pi^-\gamma$ and $q\bar{q}$ rejection	$M^2_{\text{rec}}(\pi^+\pi^-) > 4$ GeV^2

13

1   [1] Y. Sue, T. Iijima, and B. Shwartz, "Measurement of the cross section $ee \rightarrow \pi^+\pi^-\pi^0$ through
2   the radiative return method at Belle II (Internal)", .
3   [2] "Belle 2 Software Documentation", Online.
4   https://software.belle2.org/sphinx/light-2210-devonrex/analysis/doc/Variables.
5   html?highlight=cluster%20second%20moment#variable-clusterSecondMoment.